This is the accepted manuscript made available via CHORUS. The article has been published as:

Analyzing Power A_{y}(θ) of n[over →]-^{3}He Elastic Scattering between 1.60 and 5.54 MeV

J. Esterline, W. Tornow, A. Deltuva, and A. C. Fonseca

Phys. Rev. Lett. **110**, 152503 — Published 12 April 2013

DOI: 10.1103/PhysRevLett.110.152503

Analyzing Power $A_y(\theta)$ of $\vec{n}$-^{3}He Elastic Scattering between 1.60 and 5.54 MeV

J. Esterline,[1,2] W. Tornow,[1,2] A. Deltuva,[3] and A.C. Fonseca[3]

[1] *Duke University, Durham, North Carolina 27708-0308, USA*
[2] *Triangle Universities Nuclear Laboratory, Durham, North Carolina 27708-0308, USA*
[3] *Centro de Física Nuclear da Universidade de Lisboa, P-1649-003 Lisboa, Portugal*

(Dated: January 28, 2013)

Comprehensive and high-accuracy $\vec{n}$-^{3}He elastic scattering analyzing power $A_y(\theta)$ angular distributions were obtained at five incident neutron energies between 1.60 and 5.54 MeV. The data are compared to rigorous four-nucleon calculations using high-precision nucleon-nucleon potential models; three-nucleon force effects are found to be very small. The agreement between data and calculations is fair at the lower energies and becomes less satisfactory with increasing neutron energy. Comparison to p-^{3}He scattering over the same energy range exhibits unexpectedly large isospin effects.

PACS numbers: 25.40.Dn, 21.60.-n, 25.10.+s, 21.45.Ff

During the past 20 years the three-nucleon ($3N$) system was generally considered the primary laboratory to judge the quality of nucleon-nucleon (NN) potential models in non-trivial systems, and to develop and test $3N$ force (3NF) models [1, 2]. Although considerable progress has been achieved, doubts remain whether the $3N$ system alone has sufficient sensitivity for determining the role of 3NF effects in the presence of the dominant NN interaction.

The low-energy $4N$ scattering systems, which involve much more tightly bound systems than the deuteron, are expected to be a more appropriate laboratory for refining our understanding of NN forces and 3NF effects [3]. Unfortunately, so far the study of $4N$ scattering systems has not fulfilled its potential. Somewhat surprisingly, the quality and, in some cases, the lack of experimental data in the energy range accessible to rigorous $4N$ calculations have made it impossible to draw far-reaching conclusions. One exception is the high-accuracy $\vec{p}$-^{3}He scattering $A_y(\theta)$ data of Fisher *et al.* [4] in the 1.0 to 4.05 MeV energy range and of Alley *et al.* [5] at 5.54 MeV, which confirmed earlier findings [6] that the $4N$ system exhibits an $A_y(\theta)$ puzzle [7]. It is enhanced compared to the $3N$ system, although it can be emended to a larger extent than in the $3N$ systems by incorporating the 3NF at next-to-next-to-leading order (N^{2}LO) in chiral effective field theory of Navrátil [8]. This finding is in contrast to the phenomenological 3NFs TM99 [9] and URIX [10], which are quite insensitive to this observable in both systems.

Here we report on high-precision measurements of the $\vec{n}$-^{3}He $A_y(\theta)$ in the energy range between 1.60 and 5.54 MeV. This work is motivated by the lack of reliable data for the mixed-isospin $T = 0, 1$ $4N$ systems. Accurate $A_y(\theta)$ data for this reaction were not previously available at the energies of interest. In addition, the database for the $T = 0, 1$ $A_y(\theta)$ in $\vec{p}$-^{3}H scattering appears inconsistent, precluding a full assessment of the effects of isospin dependence related to $A_y(\theta)$ in the $4N$ scattering systems; these effects are notably not observable in $3N$ scattering.

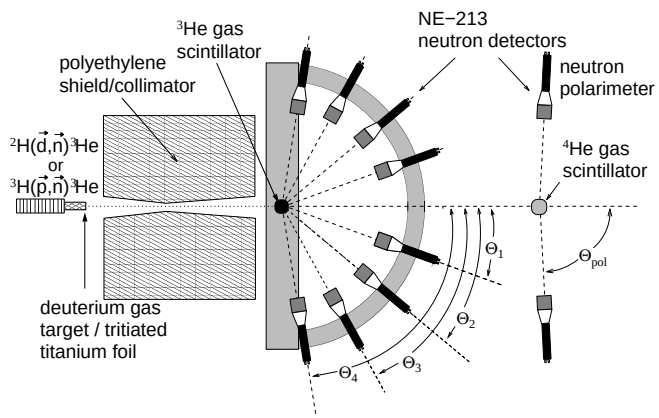

FIG. 1: Layout of experimental apparatus between neutron production and detection.

A schematic of our experimental setup at the Triangle Universities Nuclear Laboratory (TUNL) is shown in Fig. 1. An Atomic Beam Polarized Ion Source (ABPIS) [11] was used to produce either polarized proton or polarized deuteron beams with polarization axis perpendicular to the scattering plane. These beams were accelerated by TUNL's FN tandem Van de Graaff accelerator. The polarization-transfer reaction ^{3}H($\vec{p}$,$\vec{n}$)^{3}He was employed to produce polarized neutron beams at 0° with mean energies of 1.60, 2.26, and 3.14 MeV, and having energy spreads of 0.17, 0.13, and 0.11 MeV, respectively. Here, a tritiated titanium target containing 2 Ci of ^{3}H was used, and the resulting neutron polarization was typically 50%. In order to produce 4.05 and 5.54 MeV neutrons, the polarization-transfer reaction was instead ^{2}H($\vec{d}$,$\vec{n}$)^{3}He, which provided both higher neutron yield and a higher neutron polarization of typically 60%. In this case a deuterium gas cell was used with the pressure (1 or 2 atm) adjusted to limit the neutron energy spread to 0.33 MeV. The five neutron energies were cho-

sen to coincide with proton energies of the $\vec{p}$-^{3}He $A_y(\theta)$ data of [4, 5]. After passing through a collimator made of polyethylene, neutrons were scattered off ^{3}He into an array of neutron detectors mounted on a half-ring symmetrically with respect to the incident neutron beam direction. The neutron detectors consisted of rectangular liquid scintillators with neutron-gamma pulse-shape discrimination properties. The purpose of the collimator was to shield the neutron detectors from the direct illumination by the neutron source. The ^{3}He gas of 52.5 atm with a xenon admixture of 2.5 atm was contained in a high-pressure gas scintillator housing. Details about this active target are given in [12]. The center-to-center distance between the ^{3}He gas scintillator and the neutron detectors was typically 45 cm, while the center-to-center distance between the neutron source and the ^{3}He gas scintillator was 85 cm for the forward-angle geometry shown in Fig. 1, and 135 cm for the backward-angle geometry. In the latter case the half-ring was rotated in the horizontal plane through 180° after being moved downstream by 50 cm. Neutrons passing without interaction through the ^{3}He gas scintillator were scattered off ^{4}He contained in a second high-pressure gas scintillator further downstream. This active target was composed of 63 atm of ^{4}He and 5 atm of xenon gas, and, together with a pair of neutron detectors placed symmetrically with respect to the incident neutron beam direction, acted as neutron polarimeter. The two neutron detectors were identical to those employed for $\vec{n}$-^{3}He scattering, and they were positioned at angles of maximum figure-of-merit for $\vec{n}$-^{4}He scattering. Details about the neutron detectors and the polarimeter are given in [13]. In order to minimize instrumental asymmetries inherent to the $\vec{n}$-^{3}He and $\vec{n}$-^{4}He scattering assemblies, the neutron polarization direction was switched between $\hat{y}$ and $-\hat{y}$ at a frequency alternating between 10 and 5 Hz by flipping the associated proton or deuteron polarization at the ABPIS.

The data-acquisition hardware and software used to collect and analyze the present data are very similar to those of [13]. In brief, separate triggers for the $\vec{n}$-^{3}He and $\vec{n}$-^{4}He setups were formed from a coincidence between the active scatterer (^{3}He or ^{4}He gas scintillator) and, collectively, their associated neutron detectors. Data were obtained in the form of n-tuples containing, most notably, the spin polarization direction, gas scintillator pulse height, neutron detector pulse height, neutron detector pulse-shape information, and gas scintillator-to-neutron-detector time-of-flight. Data reduction consisted of applying successive single-parameter cuts. A typical neutron time-of-flight spectrum between the ^{3}He gas scintillator and a neutron detector is shown in Fig. 2 (a), with the effect of PSD being illustrated (the dashed curve corresponding to the spectrum preceding its application, the solid following). Time increases from left to right. The peak around channel 1300 is due to neutron scattering off ^{3}He, while those around channel 1000 are due to gamma-ray scattering. Cuts corresponding to the desired neutrons and the accidental background are highlighted in red (dark grey) and green (light grey), respectively. The corresponding (by color or brightness) ^{3}He recoil energy spectra are shown in Fig. 2 (b). After fitting the ^{3}He recoil peak with a skewed Gaussian, setting a cut with bounds at 5% of the pulse-height maximum, and subtracting accidentals the fully reduced n-tuple yield N_{ds} for neutron scattering with polarization direction s ($\uparrow$ or $\downarrow$) off ^{3}He into neutron detector d (**L**eft or **R**ight) was obtained. A similar procedure was followed for $\vec{n}$-^{4}He scattering. The raw analyzing power $\tilde{A}_y$ was then calculated for each scattering angle pair from the measured asymmetry via Eq. 1:

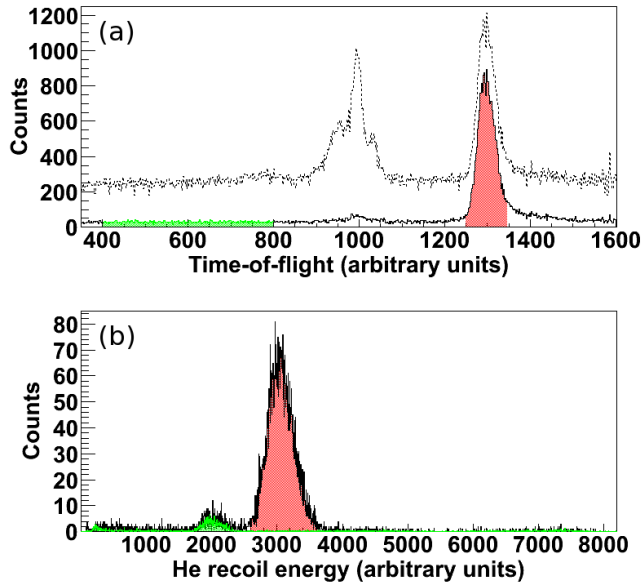

FIG. 2: (Color online) Spectra of (a) neutron time-of-flight and (b) ^{3}He recoil.

$$\epsilon = p_n \tilde{A}_y = \frac{\sqrt{N_{\mathbf{L}\uparrow} N_{\mathbf{R}\downarrow}} - \sqrt{N_{\mathbf{R}\uparrow} N_{\mathbf{L}\downarrow}}}{\sqrt{N_{\mathbf{L}\uparrow} N_{\mathbf{R}\downarrow}} + \sqrt{N_{\mathbf{R}\uparrow} N_{\mathbf{L}\downarrow}}}, \qquad (1)$$

where p_n is the neutron polarization. Eq. 1 takes advantage of the spin-flip technique to eliminate the need to determine the neutron flux and the efficiencies of the scatterer (^{3}He or ^{4}He gas scintillator) and neutron detectors. To determine p_n, Eq. 1 was first applied to the neutron polarimeter, using an effective $\vec{n}$-^{4}He $A_y(\theta)$ that we determined (following [13]) for our particular geometry via a Monte Carlo technique using the n-^{4}He phase shifts of Stammbach and Walter [14]. A very similar Monte Carlo code was employed to correct the raw $\vec{n}$-^{3}He $\tilde{A}_y(\theta)$ data for finite-geometry and multiple-scattering effects using the n-^{3}He differential cross-section R-matrix results of Hale [15], and for fiducial $A_y(\theta)$ a combination of our raw data and Hale's R-matrix predictions. In the cross-

section minimum near $\theta_{\rm c.m.} = 90° - 120°$, where corrections are largest, finite-geometry and multiple-scattering corrections were around 4% and 1%, respectively.

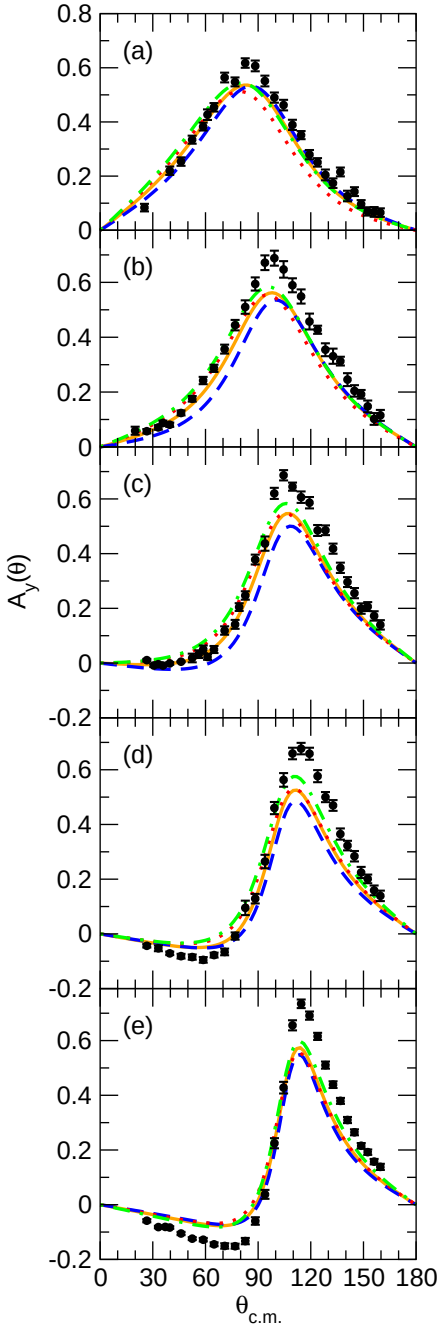

FIG. 3: Measured and calculated values of the $\vec{n}$-^{3}He analyzing power $A_y(\theta)$ at neutron energies of (a) 1.60, (b) 2.26, (c) 3.14, (d) 4.05, and (e) 5.54 MeV. Theoretical predictions using the AV18 [19], INOY04 [20], CD Bonn [21], and CD Bonn + Δ [22] potentials are shown in dashed blue, dash-dotted green, solid orange, and dotted red, respectively; experimental data are represented by black circles.

Our results for $A_y(\theta)$ and the associated statistical uncertainties are shown, along with theoretical calculations, in Fig. 3. There are between 27 and 32 data points per angular distribution, spanning the center-of-mass angular range between 27° and 159°. A total of 1.6 $\times 10^3$ hours of accelerator time was spent to accumulate these data. Systematic uncertainties include those associated with the Monte Carlo corrections and the $\vec{n}$-^{4}He $A_y(\theta)$ used to determine the neutron polarization. Both were estimated to contribute an uncertainty of 1%, absolute in the case of the former, and relative in the latter.

Regarding previous $\vec{n}$-^{3}He $A_y(\theta)$ data, the only set of importance in our energy range is that of Klages *et al.* [16] at 3.7 MeV, the maximum of whose angular distribution (of 10 data points) is about 10% lower than expected from the interpolation of our data at 3.14 and 4.05 MeV. We attribute this to the underestimation of multiple-scattering corrections in [16], where a liquid ^{3}He scintillator was used as scatterer, for which such corrections are about a factor of 10 larger than those for our ^{3}He gas scintillator.

Our theoretical description of n-^{3}He scattering is based on the Alt, Grassberger and Sandhas (AGS) equations [17] for the four-nucleon transition operators $\mathcal{U}_{\beta\alpha}$. We use the symmetrized AGS equations [3], i.e.,

$$\mathcal{U}_{11} = -P_{34}(G_0tG_0)^{-1} - P_{34}U_1G_0tG_0\mathcal{U}_{11} + U_2G_0tG_0\mathcal{U}_{21}, \tag{2a}$$

$$\mathcal{U}_{21} = (1-P_{34})(G_0tG_0)^{-1} + (1-P_{34})U_1G_0tG_0\mathcal{U}_{11}, \tag{2b}$$

where G_0 is the four free nucleon Green's function, P_{34} is the permutation operator of nucleons 3 and 4, t is the two-nucleon transition-matrix, and U_1 (U_2) is the AGS transition operator for the 3+1 (2+2) subsystem. Equations (2) are solved in the momentum-space partial-wave framework [3] where the *pp* Coulomb interaction is included using the method of screening and renormalization [18]. The n-^{3}He scattering amplitudes are given by the on-shell matrix elements of $\mathcal{U}_{11}$ calculated between the Faddeev amplitudes of the corresponding initial and final states [18].

The application of this method using different high-precision *NN* potential models (and, in one case, including a 3NF) resulted in the predictions presented in Fig. 3. The disagreement between data and calculations in the region of the $A_y(\theta)$ maximum and the emerging $A_y(\theta)$ minimum increases with incident neutron energy. AV18 [19] underestimates the data most, INOY04 [20] the least (even exceeding the data in magnitude at forward angles and low energies), while the CD Bonn [21] and CD Bonn + Δ [22] potentials give very similar predictions and tend to be intermediate in agreement (though worse than AV18 at backward angles at low energies). These degrees of accord suggest those for the ^{3}He binding energy (the measured value of which, for ease of reference, is 7.72 MeV), which is predicted variously as 6.92 (by AV18), 7.26 (CD Bonn), 7.54 (CD Bonn + Δ) and 7.73

MeV (INOY04). We thus find a partial correlation between the ^{3}He binding energy and A_y, broken by the CD Bonn + Δ model that yields an effective 3NF.

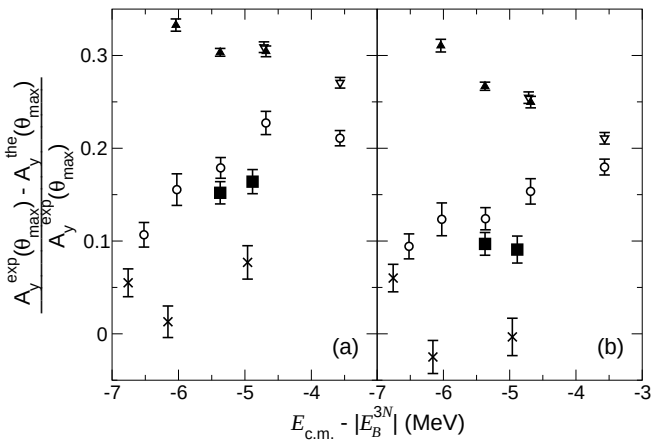

FIG. 4: A_y relative difference between measurement and calculations using (a) CD-Bonn or (b) INOY04 *NN* potentials. The total energy with respect to the four-free-nucleon threshold, given by the center-of-mass energy minus the three-nucleon bound state binding energy E_B^{3N}, provides an accurate comparison between different systems. As organized by publication, data for $\vec{p}$-^{3}He are represented by triangles filled [4] and unfilled [5], those for $\vec{p}$-^{3}H by solid squares [23] and crosses [24], and $\vec{n}$-^{3}He by open circles (the present measurements). We note the excellent agreement between [4] and [5] near -4.7 MeV resulting in an overlap.

In the absence of a more rigorous method of comparison, such as that afforded by a pending phase-shift analysis, the relative difference (RD) between the calculated and observed maxima of $A_y(\theta)$ at a given neutron energy is provided as a measure of discrepancy. RD for $4N$ systems with available $A_y(\theta)$ data are shown over the energy range of the present work in Fig. 4. While RD for the pure-isospin $T = 1$ system is very large (~ 0.3), RD for the mixed-isospin $T = 0, 1$ system $\vec{n}$-^{3}He is, surprisingly, significantly smaller and shows a completely different energy dependence, with RD decreasing with energy for $\vec{p}$-^{3}He but increasing for $\vec{n}$-^{3}He. The other mixed-isospin $T = 0, 1$ system $\vec{p}$-^{3}H represented by Kankowsky *et al.* [23] and Donoghue *et al.* [24] also yields small RD values (significantly less than 0.2, or even 0.1 for the latter set), but these data are too inconsistent to draw any conclusions on the RD energy dependence. For the mixed-isospin systems, the $T = 0$ component dominates A_y at very low energies, namely in the regime around the lowest ^{4}He P-wave resonances, especially $^3P_0$. (This accounts for the large value of the $\vec{n}$-^{3}He $A_y(\theta)$ maximum at very low energies, ~ 0.7 at $E_n = 2.26$ MeV, as compared to the $\vec{p}$-^{3}He A_y peak of ~ 0.2 at $E_p = 2.25$ MeV.) One therefore may conjecture that the $T = 0$ component is nearly correct but with increasing energy the $T = 1$ contribution to $\vec{n}$-^{3}He A_y becomes enhanced, which increases the discrepancy with the data in emulation of $\vec{p}$-^{3}He. Also, despite a recent finding [25] that the inclusion of the N^{2}LO 3NF reduces the $\vec{p}$-^{3}He A_y discrepancy by a factor of two, it is unclear to what extent this force could improve the description of $\vec{n}$-^{3}He A_y, which is known to show a different sensitivity to the interaction models—for example, the modification of *NN* P-wave potential proposed by Doleschall [20] reduces the $\vec{p}$-^{3}He A_y discrepancy by a factor of two as compared to the predictions of INOY04 but has almost no effect on $\vec{n}$-^{3}He A_y.

In conclusion, the $\vec{n}$-^{3}He $A_y(\theta)$ data and the associated calculations evince the isospin dependence of the relative difference between rigorous calculations and experimental data for $A_y(\theta)$ in the region of the A_y maximum. $A_y(\theta)$ data for $\vec{n}$-^{3}H scattering are needed to determine whether the relative difference for this pure-isospin $T = 1$ system is also very different from that of the mixed-isospin $4N$ systems. Lastly, we note that, judging from our CD-Bonn + Δ calculations, that the effective Δ-mediated 3NF contributes very little to $\vec{n}$-^{3}He $A_y(\theta)$.

The authors acknowledge valuable contributions from B.J. Crowe III, A.S. Crowell, C.R. Howell, M.R. Kiser, R.A. Macri, and R.S. Pedroni during the long data-taking phase of the experiment described in this work, which was partially supported by the U.S. Department of Energy, Office of Nuclear Physics, under Grant No. DE-FG02-97ER41033. We also thank G. Hale for providing numerical values for $\vec{p}$-^{3}H $A_y(\theta)$ data from [23] and [24].

[1] K. Sagara, Few Body Syst. **48**, 59 (2010).
[2] N. Kalantar-Nayestanaki, E. Epelbaum, J.G. Messchendorp, and A. Nogga, Rep. Prog. Phys. **75**, 016301 (2012).
[3] A. Deltuva and A.C. Fonseca, Phys. Rev. C **75**, 014005 (2007).
[4] B.M. Fisher *et al.*, Phys. Rev. C **74**, 034001 (2006).
[5] M.T. Alley and L.D. Knutson, Phys. Rev. C **48**, 1890 (1993).
[6] M. Viviani, A. Kievsky, S. Rosati, E.A. George, L.D. Knutson, Phys. Rev. Lett. **86**, 3739 (2001).
[7] A. Deltuva and A.C. Fonseca, Phys. Rev. Lett. **98**, 162502 (2007).
[8] P. Navrátil, Few-Body Syst. **41**, 117 (2007).
[9] S.A. Coon and H.K. Han, Few-Body Syst. **30**, 131 (2001).
[10] B.S. Pudliner, V.R. Pandharipande, J. Carlson, S.C. Pieper, and R.B. Wiringa, Phys. Rev. C **56**, 1720 (1997).
[11] T.B. Clegg *et al.*, NIM A **357**, 200 (1995).
[12] W. Tornow *et al.*, NIM A **647**, 86 (2011).
[13] R.T. Braun *et al.*, Phys. Lett. B **660**, 161 (2008).
[14] T. Stammbach and R.L. Walter, Nucl. Phys. A **180**, 225 (1972).
[15] G.M. Hale, private communication (2008).
[16] H.O. Klages *et al.*, Nucl. Phys. A **443** 237 (1985).
[17] P. Grassberger and W. Sandhas, Nucl. Phys. **B2**, 181 (1967); E. O. Alt, P. Grassberger, and W. Sandhas, JINR report No. E4-6688 (1972).
[18] A. Deltuva and A.C. Fonseca, Phys. Rev. C **76**, 021001(R) (2007).
[19] R.B. Wiringa, V.G.J. Stoks, and R. Schiavilla, Phys. Rev. C **51**, 38 (1995).
[20] P. Doleschall, Phys. Rev. C **69**, 054001 (2004).
[21] R. Machleidt, Phys. Rev. C **63**, 024001 (2001).
[22] A. Deltuva, R. Machleidt, and P.U. Sauer, Phys. Rev. C **68**, 024005 (2003).
[23] R. Kankowsky *et al.*, Nucl. Phys. A **263**, 29 (1976).
[24] T.R. Donoghue *et al.*, Lecture Notes in Physics **82**, 279 (1978).
[25] M.Viviani *et al.*, EPJ Web of Conferences **3**, 05011 (2010).